Role of the SPI1/CDKN2A/p53 signaling pathway in cuproptosis of lung adenocarcinoma cells

JIAYUE AN[1-3*], WEI SONG[2*], QIN WANG[2], BOYU TAN[2], XUAN FEI[2], RUOXI WANG[2], SIYAN LI[2], XIYU LU[2], YOUJIE LI[2] and NING XIE[3]

[1]Department of Clinical Laboratory, The Second Medical College of Binzhou Medical University, Yantai, Shandong 264100, P.R. China; [2]Department of Biochemistry and Molecular Biology, Binzhou Medical University, Yantai, Shandong 264003, P.R. China; [3]Department of Thoracic Surgery, Yantaishan Hospital Affiliated to Binzhou Medical University, Yantai, Shandong 264003, P.R. China

Received November 26, 2024; Accepted April 1, 2025

DOI: 10.3892/ol.2025.15099

Abstract. Lung adenocarcinoma (LUAD) is among the most prevalent malignancies worldwide. Cuproptosis, a copper-induced form of cell death, has been identified as a key process in LUAD progression; however, the molecular mechanisms underlying cuproptosis in LUAD and potential therapeutic targets remain unclear. The present study utilized The Cancer Genome Atlas database to retrieve mRNA expression profiles and clinical information of LUAD, identifying 10 candidate genes from differentially expressed genes associated with cuproptosis. Protein-protein interaction analysis indicated that CDK inhibitor 2A (CDKN2A), an upregulated gene in LUAD, may function as a hub gene. Furthermore, multiple online databases were used to analyze Spi-1 proto-oncogene (SPI1), a transcription factor upstream of CDKN2A, which was downregulated in LUAD cuproptosis. The LinkedOmics database identified the p53-mediated cuproptosis-related pathway regulated by CDKN2A. Gene expression patterns were examined through Gene Expression Profiling Interactive Analysis, the Human Protein Atlas and reverse transcription-quantitative polymerase chain reaction. Prognostic significance was assessed using the UALCAN and Kaplan-Meier plotter databases. *In vitro* experiments demonstrated that CDKN2A knockdown and SPI1 overexpression inhibited the proliferation and migration of the H1975 cell line. After copper-induced cuproptosis in H1975 cells, SPI1 expression was upregulated, whereas CDKN2A expression was downregulated. When H1975 cells were pretreated with tetrathiomolybdate, the upregulation of SPI1 was inhibited and the downregulation of CDKN2A was also suppressed. Cell Counting Kit-8 assays indicated that SPI1 overexpression and CDKN2A knockdown facilitated elesclomol-$CuCl_2$-induced cuproptosis. Western blot analysis revealed an inverse association between SPI1 overexpression and CDKN2A/p53 levels. In conclusion, the present study demonstrated the role of the SPI1/CDKN2A/p53 axis in LUAD cuproptosis, providing insights into potential therapeutic targets and contributing to clinical research on treatment strategies.

Introduction

Lung cancer is a major contributor to cancer mortality trends, with 340 people succumbing each day from lung cancer in the United States, and despite notable reductions in lung cancer-associated mortality due to early detection and therapeutic advancements, the annual mortality rate from lung cancer remains substantially higher compared with colorectal cancer, breast cancer and prostate cancer (1). Non-small-cell lung cancer (NSCLC) accounts for approximately four-fifths of all lung cancer cases (2). Lung adenocarcinoma (LUAD) is the primary histological subtype of NSCLC in terms of prevalence, followed by squamous cell carcinoma (2). Continuous advancements and innovations in medical technology have markedly improved treatment outcomes for patients with LUAD. However, when most patients are diagnosed, the disease has developed to the middle and late stages; due to the spread and metastasis of the tumor, it is difficult to achieve the ideal treatment effect, and the 5-year survival rate remains relatively low (3). Previous research has indicated that the identification and utilization of molecular biomarkers hold potential for predicting patient prognosis (4). However, a consensus on the primary drivers of LUAD has yet to be reached, and an in-depth examination into the biological characteristics and mechanisms underlying LUAD-associated genes is necessary.

Increased glycolysis in tumor cells may promote tumor growth, progression and metastasis (5). The acceleration of glucose metabolism, known as the 'Warburg effect', is crucial

Correspondence to: Dr Youjie Li, Department of Biochemistry and Molecular Biology, Binzhou Medical University, 346 Guanhai Road, Yantai, Shandong 264003, P.R. China
E-mail: youjie1979@163.com

Dr Ning Xie, Department of Thoracic Surgery, Yantaishan Hospital Affiliated to Binzhou Medical University, 10087 Keji Avenue, Yantai, Shandong 264003, P. R. China
E-mail: sunnyvvv@163.com

*Contributed equally

Key words: lung adenocarcinoma, cuproptosis, CDK inhibitor 2A, Spi-1 proto-oncogene, p53

for the conversion of pyruvic acid into lactate, and lactate derived from tumors can inhibit the tumor surveillance function of T cells and natural killer cells (5). Aerobic glycolysis and abnormal choline phospholipid metabolism are also hallmarks of cancer, and inhibiting glycolysis and choline metabolism can suppress tumor growth; regulation of cancer metabolism can occur through the crosstalk between glycolytic enzymes and phospholipid synthetases (6). Cells dependent on mitochondrial respiration are more sensitive to copper ionophores than those relying on glycolysis. Glycolysis is essential for the growth and proliferation of cancer cells; therefore, inhibiting glucose metabolism not only makes them more susceptible to treatment with the copper ionophore elesclomol (ES) but also reduces the malignant potential of these cells (7).

Tsvetkov *et al* (8) proposed a novel metal ion-mediated cell death mechanism similar to ferroptosis (9), termed copper-dependent cell death. This mechanism differs from other cell death pathways, such as apoptosis (10), pyroptosis (11) and necroptosis (12). Characterized by excessive copper binding directly to lipid-acetylated proteins of the tricarboxylic acid (TCA) cycle, this mode of cell death leads to the aggregation of lipid-acetylated proteins and subsequent destabilization of iron-sulfur (Fe-S) cluster proteins, resulting in increased protein toxic stress and ultimately cell death (8). Previous studies have reported that the direct binding of copper to the lipid-acylated components of the TCA cycle leads to TCA inhibition after pulsing with the copper ionophore ES. Metabolites related to the TCA cycle, such as citrate, cis-aconitate and guanosine diphosphate, exhibit time-dependent maladaptation, with their contents decreasing over time after ES treatment (8,13).

Previous studies have highlighted the critical role of cuproptosis-related genes (CRGs) in human cancer (8,14,15). These genes regulate copper ion transport and metabolism to maintain stable intracellular copper levels. Due to the promoting effects of copper on malignant biological behaviors, such as cell proliferation, neovascularization and tumor metastasis, the potential role of CRGs is particularly notable (16). However, the specific regulatory mechanisms of CRGs, and their effects on the progression and prognosis of LUAD remain unclear. Investigating CRGs as potential therapeutic targets may provide novel options for cancer treatment, and provides valuable insights into the molecular mechanisms underlying cancer initiation and progression.

CDK inhibitor 2A (CDKN2A) is highly expressed in most cancer types, with several genetic variations associated with patient survival and its expression (17). It resides on the p21.3 band of the short arm of human chromosome 9, exhibiting ubiquitous expression across diverse cells and tissues. It is transcribed from four exons (1α, 1β, 2 and 3), directing the synthesis of two proteins: p16INK4a (p16) and p14ARF (p14). These proteins are translated via alternative reading frames, each serving as a crucial regulator of the cell cycle (18). p16 exerts its anticancer function by maintaining the retinoblastoma protein in a hypophosphorylated state, thereby blocking cell entry into the S phase of DNA synthesis. Additionally, p14 acts as a positive regulator of p53, inhibiting MDM2 proto-oncogene (MDM2)-mediated degradation of p53. Disruption of the ability of p14 to bind MDM2 leads to MDM2-mediated degradation of p53, enabling cells to evade senescence barriers, accumulate DNA damage and facilitate tumorigenesis (19). In summary, the CDKN2A gene serves a vital role in regulating cell cycle progression and tumor suppression through its encoded proteins p16 and p14. Genetic alterations that compromise the normal functions of these proteins may disrupt cellular homeostasis and increase the risk of tumorigenesis.

As a CRG, CDKN2A, identified through whole-genome CRISPR/Cas9 knockout screens, may function as an anti-cuproptosis gene that contributes to tumor initiation and progression (8,20,21). CDKN2A acts as a negative regulator among CRGs, and its mechanism for influencing poor prognosis indicates its potential involvement in regulating cuproptosis activity (20,22). Shi *et al* (22) speculated that this might be related to the involvement of CDKN2A in the EMT process. The association of CDKN2A with most CRGs in adrenocortical carcinoma, kidney renal clear cell carcinoma, prostate adenocarcinoma and thyroid carcinoma highlights its pivotal role in cuproptosis. Pan-cancer analysis has reveal that CDKN2A expression is associated with pathological stages across multiple tumor types and is closely associated with immune infiltration, emphasizing its potential as a biomarker (23). In addition, the loss of CDKN2A function is strongly associated with the progression, prognosis and treatment of lung cancer; however, the specific mechanisms by which CDKN2A modulates cuproptosis in lung cancer remain to be clarified (24). The current lack of research elucidating the detailed mechanisms of CDKN2A in cancer cell cuproptosis presents a novel research direction for anticancer therapy and offers broad avenues for future treatment strategies.

The present study aimed to identify the hub genes associated with cuproptosis in patients with LUAD by integrating transcriptomics and clinical data from The Cancer Genome Atlas (TCGA) database. The present study aimed to comprehensively evaluate the molecular mechanisms and clinical importance of these hub genes in LUAD cuproptosis. Furthermore, validation of the findings through *in vitro* cellular experiments was performed, thereby providing novel therapeutic targets for the treatment of LUAD.

Materials and methods

Data source and preprocessing. The RNA-sequencing (RNA-seq) expression profiles of LUAD were downloaded from TCGA database (https://portal.gdc.cancer.gov) (25), comprising 530 LUAD tissue samples (T) and adjacent tissues samples from 59 patients with LUAD (N). Utilizing the rjson R package (https://github.com/alexcb/rjson) through R studio (2023.09.1 494) (26), the gene expression matrices were integrated, duplicate data were removed and gene names were converted to common identifiers, thereby acquiring LUAD-associated genes. CRGs were sourced from prior literature studies (9,14,15). SangerBox 3.0 (http://vip.sangerbox.com/) is a comprehensive, user-friendly bioinformatics analysis platform; this software was used to perform image visualization (27).

Differential expression analysis and identification of candidate LUAD CRGs. To analyze TCGA data (T=530; N=59), differential expression analysis was performed using

R packages limma-voom (28), DESeq2 (https://bioconductor.org/packages/release/bioc/html/DESeq2.html) and edgeR (https://bioconductor.org/packages/release/bioc/html/edgeR.html) to identify differentially expressed genes (DEGs) between the selected groups and their respective controls. Genes with expression values of zero in >50% of samples were excluded. To perform differential expression analysis using DESeq2 on the obtained TCGA expression dataset, the DESeqDataSetFromMatrix and DESeq functions were utilized to input the matrix and normalize the data, followed by the results function to determine the significance of differential expression for each gene. For differential expression analysis using edgeR, the DGEList and calcNormFactors functions were adopted to input the matrix and normalize the data, with the exactTest function used to assess the significance of differential expression for each gene. In the limma approach for differential expression analysis, the data were transformed using the voom function, and multivariate linear regression analysis was performed using the lmFit function. The eBayes function was then applied to calculate moderated statistical values, yielding the significance of differential expression for each gene. Hypothesis testing approaches were utilized to set P-values, false discovery rate (FDR) values and fold changes for screening DEGs. In the present study, $P<0.05$, FDR <0.05 and fold change >1.5 were applied to obtain statistically significant differences for each gene. Common DEGs from the three methods were intersected using Venn diagrams to ensure accuracy. These DEGs were then intersected with CRGs to identify 10 candidate LUAD CRGs.

Construction of protein-protein interaction (PPI) network and identification of hub genes. The STRING database (version 11.5; http://string-db.org/) (29) was employed to construct a PPI network among the differentially co-expressed genes. When constructing the gene interaction network using STRING to illustrate the PPI associations among the 10 selected genes, a confidence score of ≥0.150 was applied as the threshold. The resulting network was visualized using Cytoscape (v3.9.1) (30). Among the network analysis methods, node degree and maximal clique centrality (MCC) algorithms were applied via the cytoHubba plug-in in Cytoscape to identify potential hub nodes (31). Based on these analyses, CDKN2A, a LUAD CRG, was selected as the most credible hub gene.

Prediction of transcription factors (TFs) for target genes. A total of five databases were used to predict the potential TFs for CDKN2A and the nine other LUAD CRGs identified (AOC3, ULK2, SLC31A2, PDK1, CP, GCSH, COA6, LOXL2 and H3C1): ENCODE (https://www.encodeproject.org/), hTFtarget (http://bioinfo.life.hust.edu.cn/hTFtarget), Cistrome (http://cistrome.org/db/), TCGA-LUAD (https://portal.gdc.cancer.gov) and Genotype-Tissue Expression (GTEx) Lung (https://gtexportal.org/home). Based on Pearson correlation analysis, the correlation was calculated between the expression of target genes and TFs to ultimately obtain the required TFs. In the present study, the prediction of target gene TFs across multiple databases was performed using the website https://jingege.shinyapps.io/TF_predict/. Subsequently, the overlapping TFs predicted by ≥2 databases were identified through Venn diagrams. Among them, Spi-1 proto-oncogene (SPI1) was selected for prognostic analysis based on its prognostic significance.

Validation of gene and protein expression levels and prognostic survival value. The Gene Expression Profiling Interactive Analysis (GEPIA) 2.0 database (http://gepia.cancer-pku.cn/) (32) encapsulates a vast collection of data from 9,736 tumor samples and 8,587 normal samples sourced from TCGA and GTEx projects. In the present study, the GEPIA 2.0 database facilitated the analysis of differential gene expression levels between LUAD tissues and normal lung tissues, as well as correlations among genes. The Human Protein Atlas 24.0 (HPA 24.0; images available from v24.proteinatlas.org) (33) was utilized to further corroborate the protein expression levels of specific genes in LUAD vs. normal lung tissues by visually inspecting the protein expression of relevant genes in pathological sections of normal lung and LUAD tissues, thereby verifying the differences in protein expression.

The UALCAN database (http://ualcan.path.uab.edu/) (34), an online analysis and mining tool based on TCGA data, was used to verify the reliability of hub genes by analyzing the differences in mRNA expression levels between LUAD tissues and normal tissues, as well as their prognostic significance. Additionally, the Kaplan-Meier (KM) plotter database (http://kmplot.com/analysis/) (35) was employed to examine the effect of gene expression on overall survival (OS), first progression (FP) and post-progression survival (PPS) in patients with LUAD; the patients were divided according to median values, and the dataset names were 211156-at, 207039-at and 209644-at. The test method used log-rank test to compare between groups and to calculate P-values, and then Cox multivariate analysis was performed to calculate the hazard ratio to determine the independent prognostic role of genes; the follow-up threshold was 120 months.

Exploration of co-expression networks and gene enrichment analysis. LinkedOmics 1.2 (http://www.linkedomics.org/login.php) (36), a visualization platform, was used to explore gene expression profiles. Using LinkedOmics, co-expressed genes of CDKN2A were identified through Spearman's correlation coefficient analysis. The results were visualized using heatmaps and volcano plots. Subsequently, Gene Set Enrichment Analysis was performed to investigate the Gene Ontology (GO) terms and Kyoto Encyclopedia of Genes and Genomes (KEGG) pathways associated with CDKN2A and its co-expressed genes. The data were downloaded from LinkedOmics and used HelixLife 2.0.28 (https://www.helixlife.cn/) to visualize the GO graph. The KEGG database (https://www.genome.jp/kegg/) (37), which interconnects disease genes, pathways, drugs and diagnostic markers, served as the primary resource for signal pathway enrichment analysis.

Evaluation of the statistical significance of core genes. To assess the credibility of core genes, the normal dataset (accession number: 000319563900002) from GTEx was incorporated into the present analysis. A comprehensive analysis of RNA-seq data in transcripts per million format was performed from TCGA and GTEx, which were uniformly processed using the Toil pipeline, in the University of California Santa Cruz Xena database (https://xenabrowser.net/datapages/) (38). The final

Table I. Plasmid information.

Transfection vector	Plasmid backbone and catalog number	Sequence, 5'-3'
sh-CDKN2A	pLV3-U6-CDKN2A(human)-shRNA1-Puro (cat. no. P49363)	GCUCUGAGAAACCUCGGGAAACUC GAGUUUCCCGAGGUUUCUCAGAGC
sh-NC	pLKO.1-puro (cat. no. P0258)	
oe-SPI1	pCMV-3xFLAG-SPI1(human)-EGFP-Neo (cat. no. P52919)	
oe-NC	pCMV-3xFLAG-MCS-EGFP-Neo (cat. no. P46073)	

All plasmids were purchased from Wuhan MiaoLing Biotech Science Co., Ltd. sh, short hairpin; NC, negative control; oe, overexpression; CDKN2A, CDK inhibitor 2A; SPI1, Spi-1 proto-oncogene.

analysis included 515 LUAD samples from TCGA, as well as 59 normal tissue samples from TCGA and an additional 288 normal tissue samples from GTEx. The Wilcoxon rank-sum test was selected for statistical analysis, and the ggplot2 3.4.4 package (https://ggplot2.tidyverse.org) was utilized for data visualization to validate the significance of the core genes.

Cell transfection. The normal human lung epithelial BEAS-2B cell line and the LUAD H1975 cell line were obtained from The Cell Bank of Type Culture Collection of The Chinese Academy of Sciences. Cells in the logarithmic growth phase were seeded into 6-well plates containing RPMI-1640 (cat. no. PM150110; Wuhan Pricella Biotechnology Co., Ltd.; Wuhan Elabscience Biotechnology Co., Ltd.) medium supplemented with 10% fetal bovine serum (Wuhan Pricella Biotechnology Co., Ltd.; Wuhan Elabscience Biotechnology Co., Ltd.) and 1% penicillin-streptomycin (Beyotime Institute of Biotechnology). When the cells reached 60-70% confluence, plasmids (1.5 μg) were transfected into the cells using Lipofectamine® 2000 (Thermo Fisher Scientific, Inc.). The transfection ratio was 1:1.5, Lipofectamine 2000:plasmid. The plasmid backbone names and sequences are presented in Table I. The short hairpin (sh)RNA-CDKN2A (sh-CDKN2A), sh-negative control (NC; empty plasmid), overexpression (oe)-SPI1 and oe-NC (empty plasmid) plasmids (1.5 μg) were transfected into the H1975 cell line and cultured at 37˚C in a 5% CO_2 incubator for 48 h. The transfection efficiency was assessed by reverse transcription-quantitative polymerase chain reaction (RT-qPCR).

RT-qPCR analysis. Total RNA was extracted from BEAS-2B and H1975 cells using RNAiso Plus (cat. no. 9109; Takara Bio, Inc.) and RNA concentrations were quantified with an ultra-micro spectrophotometer. According to the manufacturer's protocol, RT of RNA was performed using HiScript II Q RT SuperMix for qPCR (+gDNA wiper; cat. no. R223; Vazyme Biotech Co., Ltd.). SYBR qPCR Master Mix (cat. no. Q311; Vazyme Biotech Co., Ltd.) was used for qPCR analysis. According to the manufacturer's protocol the following thermocycling conditions were performed: Pre-denaturation at 95˚C for 30 sec; followed by 40 cycles of denaturation at 95˚C for 10 sec, annealing at 60˚C for 30 sec and extension at 72˚C for 30 sec. Relative gene expression levels were analyzed using the $2^{-\Delta\Delta Ct}$ method (39). GAPDH served as the internal reference gene with the following primer sequences: Forward, 5'-TGCACCACCAACTGCTTAGC-3' and reverse, 5'-GGCATGGACTGTGGTCATGAG-3'. The primer sequences for CDKN2A were: Forward, 5'-CTTCCTCGGGTGCCGATAC-3' and reverse, 5'-ACCCCTTCATTGCTACTCGAT-3'. For SPI1, the primer sequences were: Forward, 5'-GTGCCCTATGACACGGATCTA-3' and reverse, 5'-AGTCCCAGTAATGGTCGCTAT-3'.

Western blot analysis. Transfected cells were lysed on ice using RIPA lysis buffer (Beyotime Institute of Biotechnology) to extract proteins, and protein concentration was determined using the BCA kit (cat. no. P0012; Beyotime Institute of Biotechnology). Proteins (20 μg) were subjected to sodium dodecyl sulfate-polyacrylamide gel electrophoresis on a 12% gel and transferred to a PVDF membrane using conventional wet transfer methods. The membrane was blocked with 5% skimmed milk powder in TBS-0.1% Tween (TBST) at room temperature for 2 h. An overnight incubation with primary antibodies at 4˚C followed. The next day, the membrane was washed three times with TBST and incubated with secondary antibodies for 2 h at 4˚C. After another three washes with TBST, enhanced chemiluminescence solution (Biosharp Life Sciences) was added for exposure. ImageJ software (1.54f; National Institutes of Health) was used to measure the gray values of each band, with GAPDH serving as the internal control. Relative protein expression levels were semi-quantified as the ratio of gray values of the target protein to gray values of GAPDH. The antibodies used were in the present study were as follows: Rabbit anti-CDKN2A antibody (1:1,000; cat. no. BS40808; Bioworld Technology, Inc.), rabbit anti-p53 antibody (1:2,000; cat. no. 21891-1-AP; Proteintech Group, Inc.), rabbit anti-GAPDH antibody (1:3,000; cat. no. AP0063; Bioworld Technology, Inc.) and a Goat Anti-Rabbit IgG secondary antibody (1:6,000; cat. no. BS13278; Bioworld Technology, Inc.).

Cell Counting Kit-8 (CCK-8) assay. Cell viability was assessed using the CCK-8 assay kit (Wuhan Elabscience Biotechnology Co., Ltd.). Transfected H1975 cells (sh-NC, sh-CDKN2A, oe-NC and oe-SPI1) were seeded into 96-well plates at a

density of $2x10^3$ cells/well and incubated at 37˚C. Each group contained four replicate wells. The cells were incubated for 0, 24, 48 and 72 h, with 10 μl CCK-8 solution added to each well at each time point, followed by 2 h incubation. Absorbance at 450 nm was measured using a microplate reader.

Wound healing assay for cell migration. Cells transfected with sh-NC, sh-CDKN2A, oe-NC and oe-SPI1 were seeded into 6-well plates at a density of $5x10^5$ cells/well and cultured to form a monolayer. A scratch was created using a 10-μl pipette tip, and the cells were maintained in RPMI-1640 medium containing 1% FBS. The scratch area was observed and images were captured using an optical microscope at 0, 24 and 48 h. The scratch areas were marked using Photoshop software (version 23.0.0; Adobe Systems, Inc.).

Establishment of a cuproptosis model. The LUAD cell line H1975 was selected and maintained in RPMI-1640 medium under standard humidified incubator conditions at 37˚C with 5% CO_2. Three distinct groups were established within the experiment: A control group, an ES-$CuCl_2$ group and a tetrathiomolybdate (TTM)-ES-$CuCl_2$ group. ES, an efficacious Cu^{2+} ionophore that enhances cellular apoptosis, was sourced from MedChemExpress. TTM, a copper chelator that functions as a copper antagonist, was procured from Shanghai Yuanye Biotechnology Co., Ltd. ES was dissolved in 100% dimethyl sulfoxide (Beijing Solarbio Science & Technology Co., Ltd.) and the control group was treated with an equal amount of dimethyl sulfoxide. $CuCl_2$ (Shanghai Macklin Biochemical Co., Ltd.) was dissolved in sterile water. ES-$CuCl_2$ was prepared by mixing ES and $CuCl_2$ in a 1:1 ratio. In the ES-$CuCl_2$ group, H1975 cells were treated with 30 nM ES-$CuCl_2$ for 2 h. By comparison, cells in the TTM-ES-$CuCl_2$ group were pretreated overnight with 20 μM TTM before exposure to 30 nM ES-$CuCl_2$ for 2 h. After the aforementioned treatment, the cells of each group were cultured in fresh medium at 37˚C and 5% CO_2 for 48 h, and RNA was extracted. Gene expression was quantitatively detected by RT-qPCR.

Statistical analysis. For gene pathway analysis (n=515) and core gene validation and correlation analysis (T=483; N=347), Pearson correlation analysis was used. When analyzing the gene expression differences between the normal group and the cancer group (T=483, N=347) using the GEPIA database, an independent samples t-test was employed. When comparing differences between normal and cancer groups in both TCGA and GTEx datasets (T=515; N=347), non-parametric Wilcoxon rank-sum test were performed, using disease status as the variable for calculating differential expression. For patient survival analysis, the log-rank test and Cox univariate regression were utilized. In experimental validation, differences between groups were assessed using one-way ANOVA with Tukey's post hoc test. A unpaired Student's t-test was used to compare differences between two groups. Results are expressed as the mean ± standard deviation. P<0.05 was considered to indicate a statistically significant difference. All calculated results were statistically analyzed using GraphPad Prism 9.1 software (Dotmatics). All experiments were repeated three times.

Results

Identification of CRGs in patients with LUAD from TCGA. Differential gene expression analysis was performed on 59,427 genes associated with LUAD, retrieved from TCGA database using the R packages limma-voom, DESeq2 and edgeR. The datasets employed in all three methods excluded genes with >50% zero expression values from TCGA dataset. All analyses were executed within the SangerBox software platform. Genes with P<0.05, FDR <0.05 and fold change >1.5 were selected and sorted based on their P-values. According to the limma-voom method, 13,651 significantly DEGs were identified between LUAD and normal lung tissues (Fig. 1A). A total of 16,559 DEGs were detected using DESeq2 (Fig. 1B), whereas edgeR analysis yielded 12,151 DEGs (Fig. 1C). The intersection of these three gene sets revealed 10,252 common DEGs (Fig. 1D). These common DEGs were subsequently intersected with a set of 45 CRGs derived from the literature (Fig. 1E), resulting in 10 candidate genes (Fig. 1F). Among these candidates, three genes (AOC3, ULK2 and SLC31A2) were downregulated, whereas seven genes (PDK1, CP, GCSH, COA6, LOXL2, CDKN2A and H3C1) were upregulated (Fig. 1G). The statistical values associated with genes in the heatmap all adhered to P<0.05, FDR <0.05 and fold change >1.5.

Hub gene selection and prognostic significance analysis. The STRING database was utilized to investigate potential interactions among candidate genes, and the results were visualized using Cytoscape. A PPI network was constructed by importing 10 candidate genes into the STRING database, which expanded to 15 nodes and 34 edges (Fig. 2A). Hub genes were identified using the MCC algorithm from the cytoHubba plug-in within Cytoscape. Genes with high scores are represented by red nodes, whereas those with low scores are denoted by yellow nodes (Fig. 2B). Based on image analysis, the LUAD CRG CDKN2A, with a score of 252, was selected as the hub gene for further investigation (Fig. 2C). The UALCAN database was employed to predict the effect of CDKN2A expression on OS of patients with LUAD, samples were categorized into two groups: High-expression (with TPM values above upper quartile) and low/medium expression (with TPM values below upper quartile), revealing that patients in the CDKN2A high-expression group exhibited worse OS compared with the low/medium expression-group (P=0.0023; Fig. 2D). The KM plotter database was used to assess the influence of CDKN2A (also known as multiple tumor suppressor 1) expression on OS, PPS and FP in LUAD, thereby validating the findings (Fig. 2E-M). The results indicated that of the nine datasets analyzed, only two showed non-significant PPS (P=0.14, Fig. 2H; P=0.1, Fig. 2J), whereas all other datasets demonstrated statistical significance (P<0.05). Due to the relatively small sample size of ~300 cases for PPS compared with ~1,000 cases for OS and FP, there may be potential biases or errors in the PPS results. Nevertheless, high CDKN2A expression was associated with unfavorable patient prognosis, which supports the potential of CDKN2A levels as a predictive marker for long-term survival in patients with LUAD.

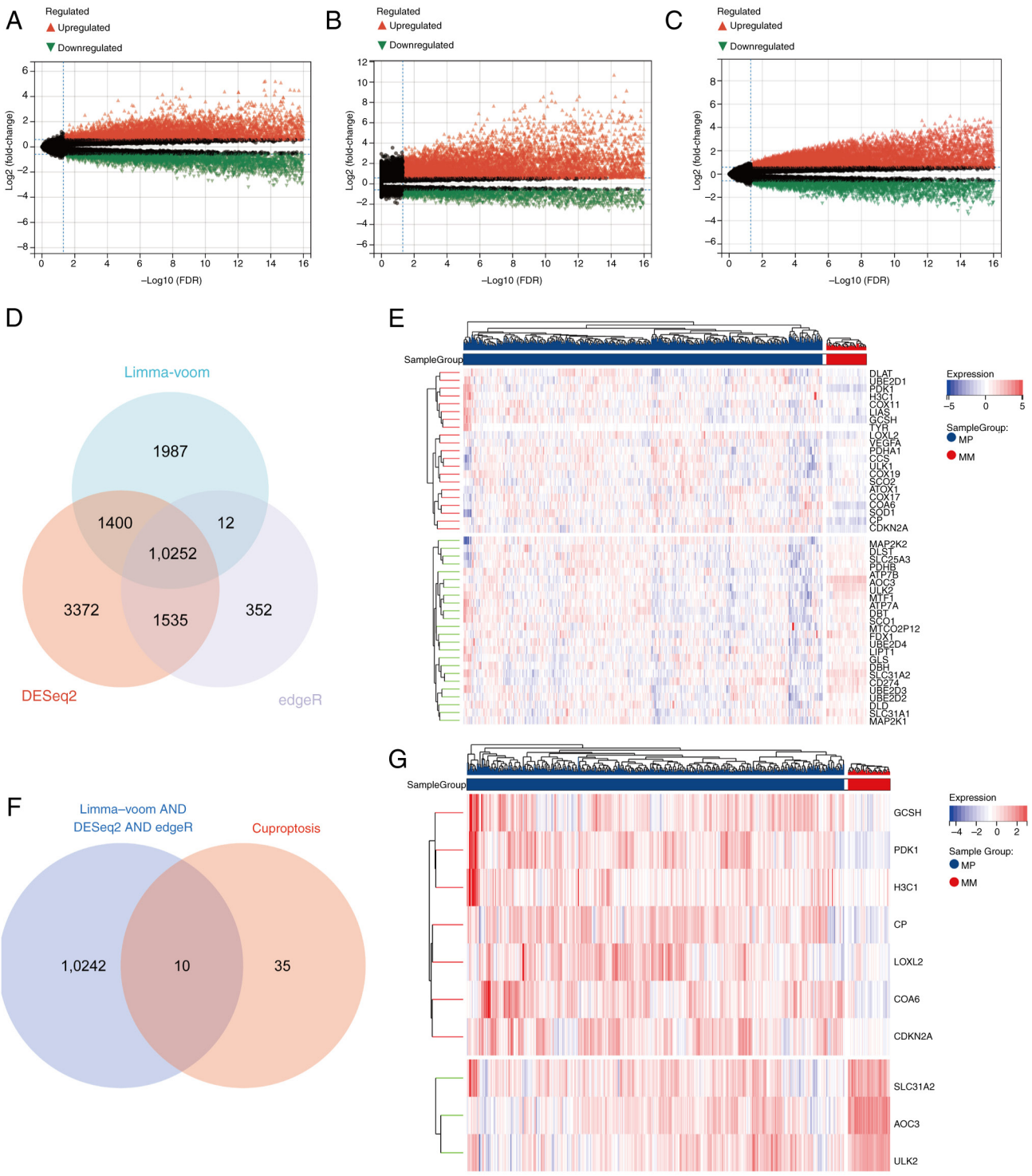

Figure 1. Identification of CRGs in LUAD. (A) Volcano plot generated using the limma-voom package depicting 13,651 DEGs between normal lung tissues (n=59) and LUAD tissues (n=530). (B) Volcano plot from the DESeq2 package illustrated 16,559 DEGs between normal lung and LUAD tissues. (C) Volcano plot generated using the edgeR package identified 12,151 DEGs between normal lung and LUAD tissues. (D) A Venn diagram representing the intersection of 10,252 common DEGs identified in LUAD. (E) A heatmap presenting 45 previously reported CRGs; MM refers to normal lung tissues and MP refers to LUAD tissues. (F) A Venn diagram depicting the intersection of CRGs with the LUAD DEGs, revealing common candidate genes. (G) A heatmap illustrating the expression patterns of 10 cuproptosis-related candidate genes in the TCGA-LUAD samples. CRGs, cuproptosis-related genes; LUAD, lung adenocarcinoma; DEGs, differentially expressed genes; FDR, false discovery rate.

Knockdown of CDKN2A inhibits proliferation and migration of LUAD cells. The GEPIA database predicted the clinical specimen tissue expression levels of CDKN2A between LUAD tissues and normal tissues. The results indicated that CDKN2A was significantly upregulated in LUAD tissues compared with in normal tissues (Fig. 3A). RT-qPCR validation revealed that the mRNA expression levels of CDKN2A in H1975 cells were significantly higher compared with those in BEAS-2B cells (Fig. 3B). The HPA database was utilized to assess and verify the presence of protein differences between normal lung tissues

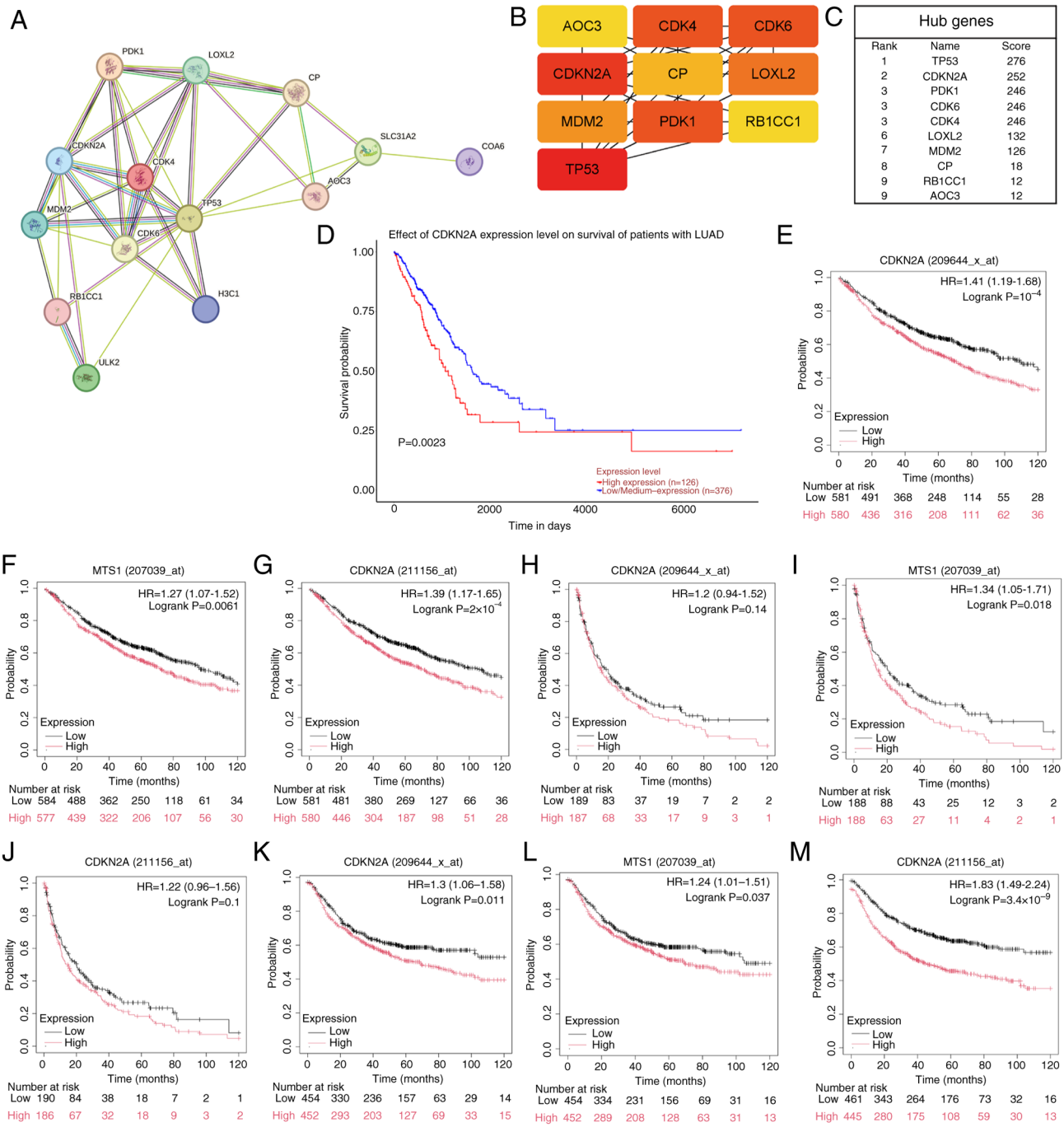

Figure 2. A PPI network constructed to identify hub genes and analyze their prognostic significance. (A) An expanded PPI network centered on 10 overlapping genes was constructed using the STRING database, comprising 15 nodes and 34 edges. (B) Pivotal genes within the PPI network were identified using the maximal clique centrality algorithm. Genes with high scores are represented by red nodes (TP53, CDKN2A, PDK1, CDK6, CDK4), and those with low scores are depicted in yellow (LOXL2, MDM2, CP, RB1CC1, AOC3). (C) As one of the 10 candidate genes for cuproptosis in LUAD cells, CDKN2A was a gene with a high score and was thus selected as the hub gene. (D) Survival analysis of OS in The Cancer Genome Atlas-LUAD cohort focused on CDKN2A (high, n=126; low n=376). (E-G) KM plotter analysis revealed an association between high expression levels of CDKN2A and poor OS. (H-J) Elevated expression of CDKN2A predicted adverse progression-free survival, as evidenced by the KM plotter analysis. (K-M) High expression of CDKN2A indicated unfavorable first progression, as illustrated through the KM plotter analysis. KM, Kaplan-Meier; PPI, protein-protein interaction; OS, overall survival; LUAD, lung adenocarcinoma; CDKN2A, CDK inhibitor 2A; HR, hazard ratio; MTS1, multiple tumor suppressor 1.

and LUAD tissues for CDKN2A, further confirming its role in LUAD tissues; the results revealed that CDKN2A protein expression was increased in LUAD tissues than in normal tissues (Fig. 3C). Following the knockdown of CDKN2A in H1975 cells using sh-CDKN2A, RT-qPCR validation of knockdown efficiency demonstrated that the expression levels of CDKN2A in the sh-CDKN2A group were significantly lower compared with those in the sh-NC group (Fig. 3D). The CCK-8 assay showed that CDKN2A knockdown inhibited cell proliferation (Fig. 3E). The wound healing assay assessing cell migration demonstrated reduced migratory ability of H1975 cells after CDKN2A knockdown (Fig. 3F). These findings indicated that CDKN2A knockdown may inhibit the proliferative and migratory capacity of H1975 cells.

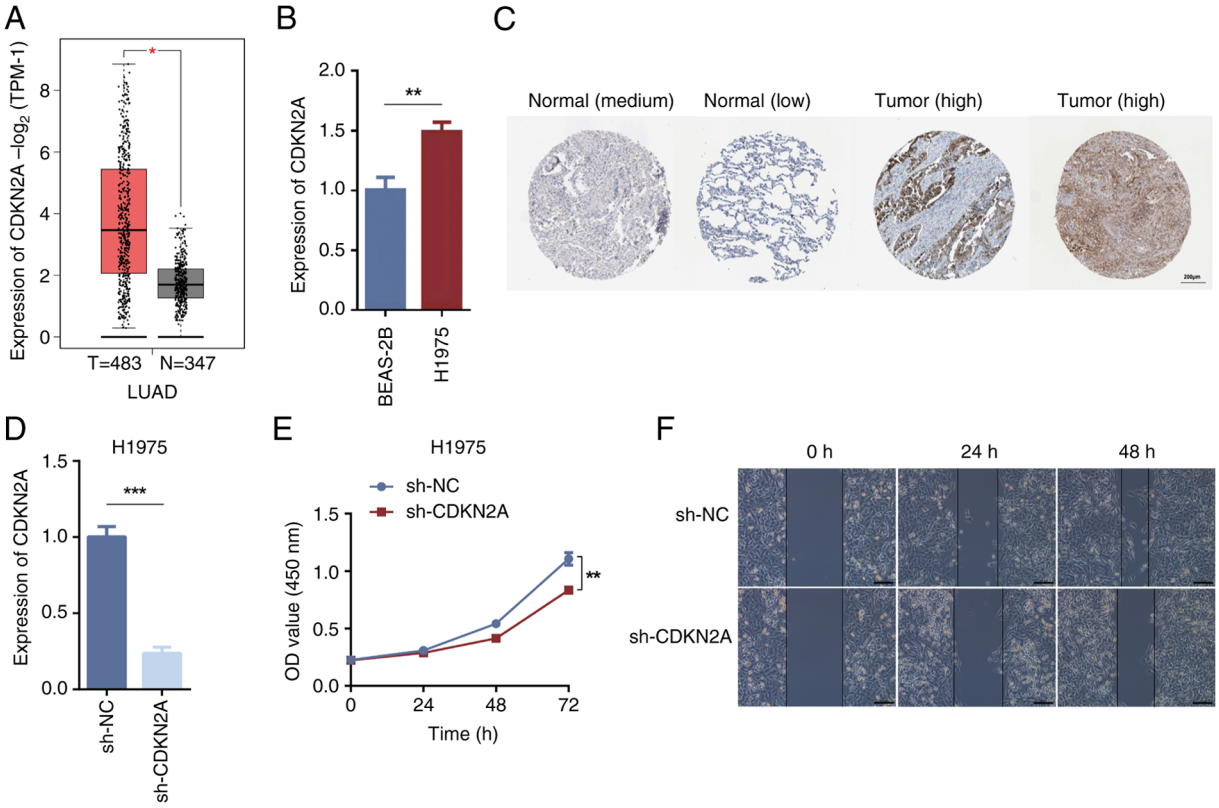

Figure 3. Knockdown of CDKN2A significantly inhibits proliferation and migration in LUAD. (A) GEPIA database was utilized to predict the expression levels of CDKN2A in tumor (n=483) and normal tissues (n=347) of patients with LUAD. (B) RT-qPCR validated the expression of the hub gene, CDKN2A, in normal and LUAD cell lines. (C) Immunohistochemistry images available from the Human Protein Atlas database demonstrated differences in the protein expression of CDKN2A between normal and LUAD tissues (images available from v24.proteinatlas.org). (D) RT-qPCR was employed to detect transfection efficiency in cells after the knockdown of CDKN2A. (E) Proliferative capability of H1975 cells after the knockdown of CDKN2A was assessed using the Cell Counting Kit-8 assay. (F) Wound healing assay revealed that the knockdown of CDKN2A inhibited the migration of the H1975 tumor cell line. *P<0.05; **P<0.01, ***P<0.001. CDKN2A, CDK inhibitor 2A; LUAD, lung adenocarcinoma; RT-qPCR, reverse transcription-quantitative polymerase chain reaction; sh, short hairpin; NC, negative control; OD, optical density.

Co-expression network and gene enrichment analysis of CDKN2A in LUAD. To investigate the potential functions and mechanisms of CDKN2A in LUAD, analysis of CDKN2A co-expressed genes was performed using LinkedOmics on RNA-seq data from patients with LUAD in TCGA database. The resulting gene correlation heatmap analysis revealed that CDKN2A expression was positively correlated with the top 50 genes, including MTAP, CDKN2B, CCNE1 and RFC4 (Fig. 4A), and was negatively correlated with the top 50 genes, such as EPAS1, ATF7, MTUS1 and SIAE (Fig. 4B). Subsequently, the KEGG pathways and GO terms enriched in the co-expressed genes of CDKN2A were analyzed. The KEGG pathway analysis indicated that the co-expressed genes of CDKN2A primarily participated in the 'cell cycle', 'DNA replication', 'p53 signaling pathway' and 'cAMP signaling pathway' (Fig. 4C), All mentioned KEGG pathways were P<0.05. The GO functional analysis revealed that CDKN2A co-expressed genes participated in biological processes such as 'DNA replication' and 'DNA-templated DNA replication'; cellular components such as 'nuclear chromosome', 'chromosomal region' and 'spindle'; and molecular functions including 'catalytic activity, acting on DNA', 'protein kinase regulator activity' and 'single-stranded DNA binding' (Fig. 4D). All mentioned GO terms were P<0.05. The p53 pathway related to cuproptosis was selected for further study with FDR<0.05. Further exploration of the KEGG database demonstrated that CDKN2A exerts its effects by regulating different genes through the p53 pathway (Fig. 4E).

SPI1 regulates CDKN2A to affect cuproptosis in LUAD cells. Utilizing the hTFtarget database, 17 potential co-TFs were predicted for nine CRGs, including AOC3, ULK2, SLC31A2, PDK1, CP, GCSH, COA6, LOXL2 and H3C1 (Fig. 5A). A total of 25 common TFs were identified for CDKN2A by integrating data from the ENCODE, hTFtarget, Cistrome, TCGA-LUAD and GTEx Lung databases (Fig. 5B). The intersection of these two predicted TF sets suggested that SPI1 and SRF might serve roles in the transcriptional regulation of CDKN2A (Fig. 5C). Prognostic survival analysis of SPI1 and SRF using the UALCAN database revealed that SRF did not show prognostic significance (P=0.74; Fig. 5D). By contrast, the prognostic survival analysis of SPI1 revealed a statistically significant difference between the high and low expression groups; notably, the prognosis of the low expression group was poor (P=0.016; Fig. 5E).

Overexpression of SPI1 inhibits proliferation and migration in LUAD cells. The tissue expression level predictions from clinical specimens revealed significant differences in SPI1 expression between normal and LUAD tissues, with LUAD

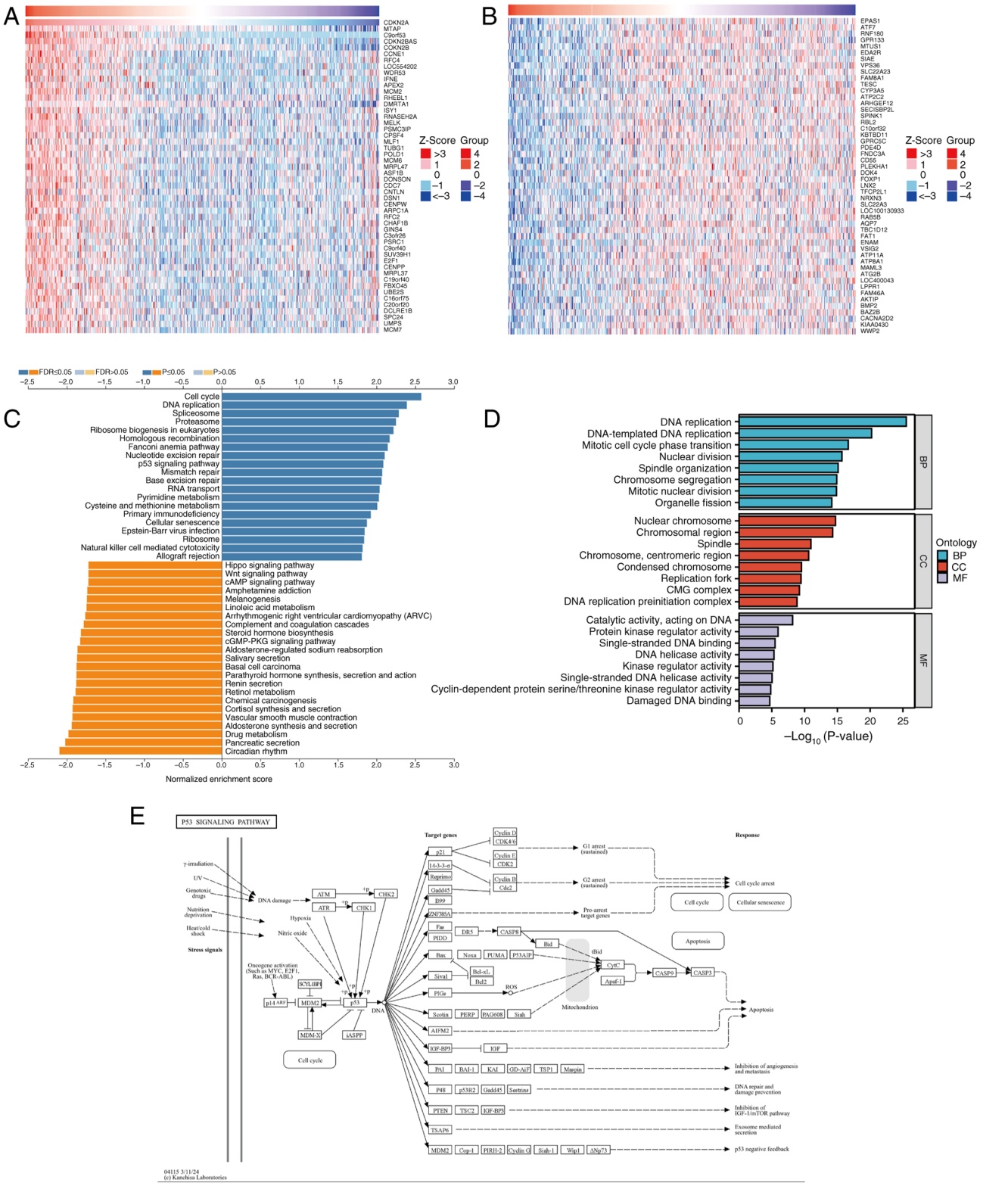

Figure 4. Co-expression network and potential functions of CDKN2A in LUAD samples (n=515). The top 50 (A) positively and (B) negatively correlated genes with CDKN2A expression in LUAD. (C) KEGG pathway analysis of CDKN2A-associated genes in LUAD. (D) Gene Ontology analysis of CDKN2A-associated genes in LUAD. (E) KEGG database prediction of relevant pathways and genes where CDKN2A (p14ARF) influences the p53 pathway. CDKN2A, CDK inhibitor 2A; LUAD, lung adenocarcinoma; KEGG, Kyoto Encyclopedia of Genes and Genomes.

tissues exhibiting lower SPI1 expression levels compared with normal tissues (Fig. 6A). RT-qPCR validation demonstrated that SPI1 expression in H1975 cells was significantly lower compared with that in BEAS-2B cells (Fig. 6B). Furthermore, the HPA database was utilized to assess and validate the differential SPI1 protein levels between normal lung tissues and LUAD tissues, highlighting its role in LUAD; the results indicated that SPI1 protein expression was lower in LUAD

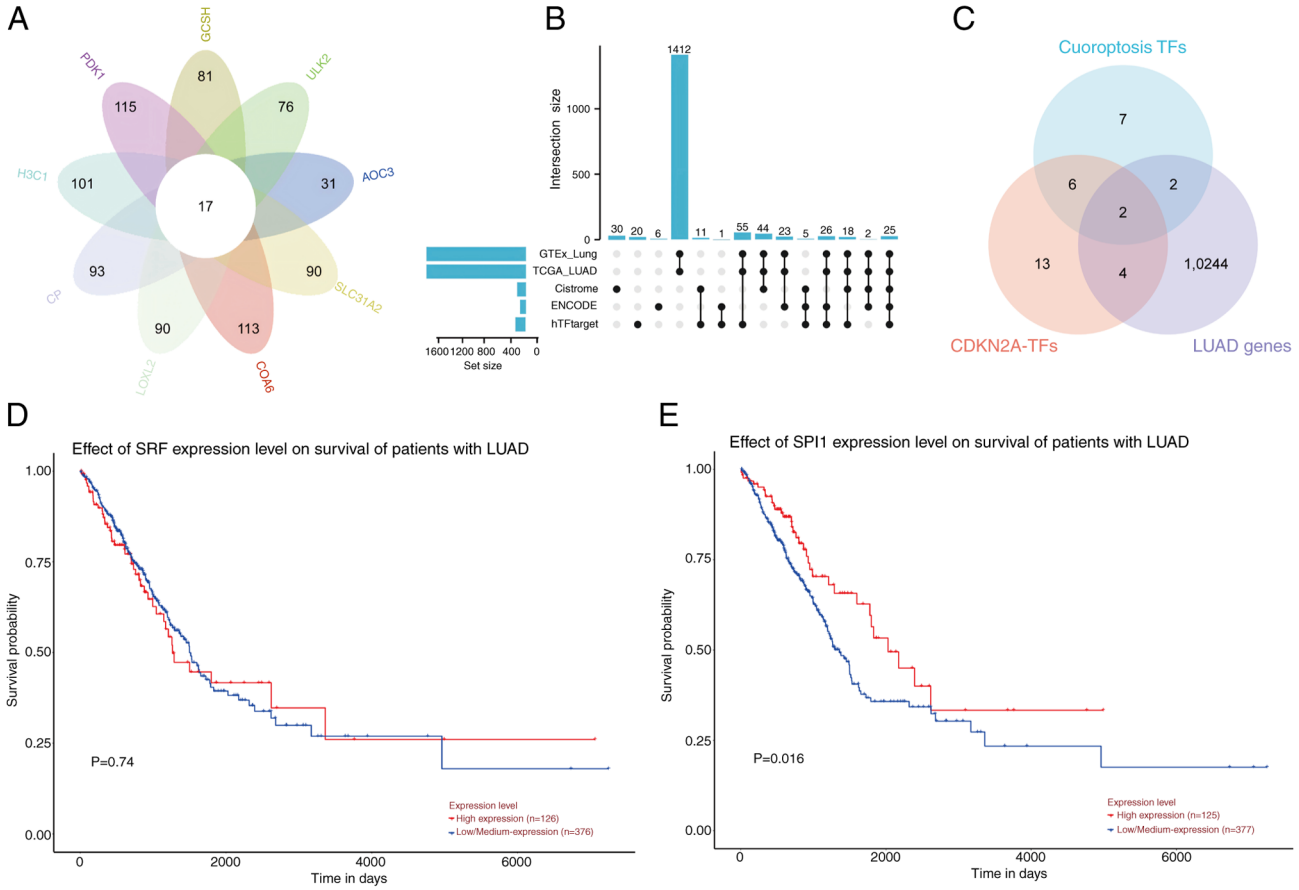

Figure 5. SPI1 regulates CDKN2A expression to affect cuproptosis in LUAD cells. (A) Venn diagram of potential upstream TFs for CRGs. (B) UpSet plot displaying the 25 potential TFs regulating CDKN2A in LUAD by different databases. (C) Venn diagram of potential TFs of CRGs and CDKN2A in LUAD. (D) OS analysis of SRF expression in LUAD, with P>0.05 indicating no statistical significance (high, n=126; low, n=376). (E) OS analysis of SPI1 expression in LUAD, with P<0.05 indicating statistical significance (high, n=125; low, n=377). SPI1, Spi-1 proto-oncogene; CDKN2A, CDK inhibitor 2A; LUAD, lung adenocarcinoma; TFs, transcription factors; CRGs, cuproptosis-related genes; OS, overall survival; TCGA, The Cancer Genome Atlas.

tissues than in normal tissues (Fig. 6C). Following the overexpression of SPI1 in H1975 cells using oe-SPI1, RT-qPCR analysis revealed a significant increase in SPI1 expression levels in the oe-SPI1 group compared with those in the oe-NC group (Fig. 6D). CCK-8 assays evaluating cell viability indicated that SPI1 overexpression inhibited cell proliferation (Fig. 6E). Wound healing assays assessing cell migration demonstrated reduced migration of H1975 cells in the oe-SPI1 group compared with that in the oe-NC group (Fig. 6F). These findings indicated that high SPI1 expression may inhibit cell proliferation and migration.

Overexpression of SPI1 and knockdown of CDKN2A sensitizes LUAD cells to cuproptosis inducers. A cuproptosis induction model was established (Fig. 7A) to investigate whether the expression of SPI1 and CDKN2A is influenced by cuproptosis. The results indicated that ES-$CuCl_2$ induced cuproptosis leading to significant upregulation of SPI1 expression and downregulation of CDKN2A expression. However, when H1975 cells were pretreated with TTM, the upregulation of SPI1 was inhibited and the downregulation of CDKN2A was also suppressed (Fig. 7B). Furthermore, the sensitivity of H1975 cells to cuproptosis activators was assessed after knocking down CDKN2A or overexpressing SPI1 to explore the roles of SPI1 and CDKN2A in LUAD cuproptosis. CCK-8 assay results demonstrated that SPI1 overexpression (Fig. 7C) and CDKN2A knockdown (Fig. 7D) promoted ES-$CuCl_2$-induced cuproptosis in H1975 cells.

SPI1/CDKN2A/p53 signaling pathway regulates cuproptosis in LUAD cells. Through integrated analysis of lung tissue data from TCGA-GTEx, boxplots showed statistically significant differences in SPI1 (Fig. 8A), CDKN2A (Fig. 8B) and TP53 (Fig. 8C) expression (P<0.001) between normal lung tissues and LUAD tissues. The expression levels of SPI1 were significantly lower in LUAD tissues than those in normal tissues, whereas the expression levels of CDKN2A and p53 were significantly higher in LUAD tissues than those in normal tissues. The GEPIA database was used to predict the correlations between genes to demonstrate the regulatory association within the SPI1/CDKN2A/p53 signaling axis. The results showed that SPI1, as a TF, was negatively correlated with CDKN2A (P<0.01; Fig. 8D) and TP53 (P<0.01; Fig. 8E), whereas CDKN2A was positively correlated with TP53 (P<0.01; Fig. 8F). Notably, the correlations between SPI1 and CDKN2A, and between CDKN2A and p53 were considered weak (r-values <0.3/-0.3). Therefore, western blot analysis was performed for verification. The overexpression of SPI1 in H1975 cells resulted in decreased protein levels of CDKN2A and p53 (Fig. 8G), and the knockdown of CDKN2A decreased

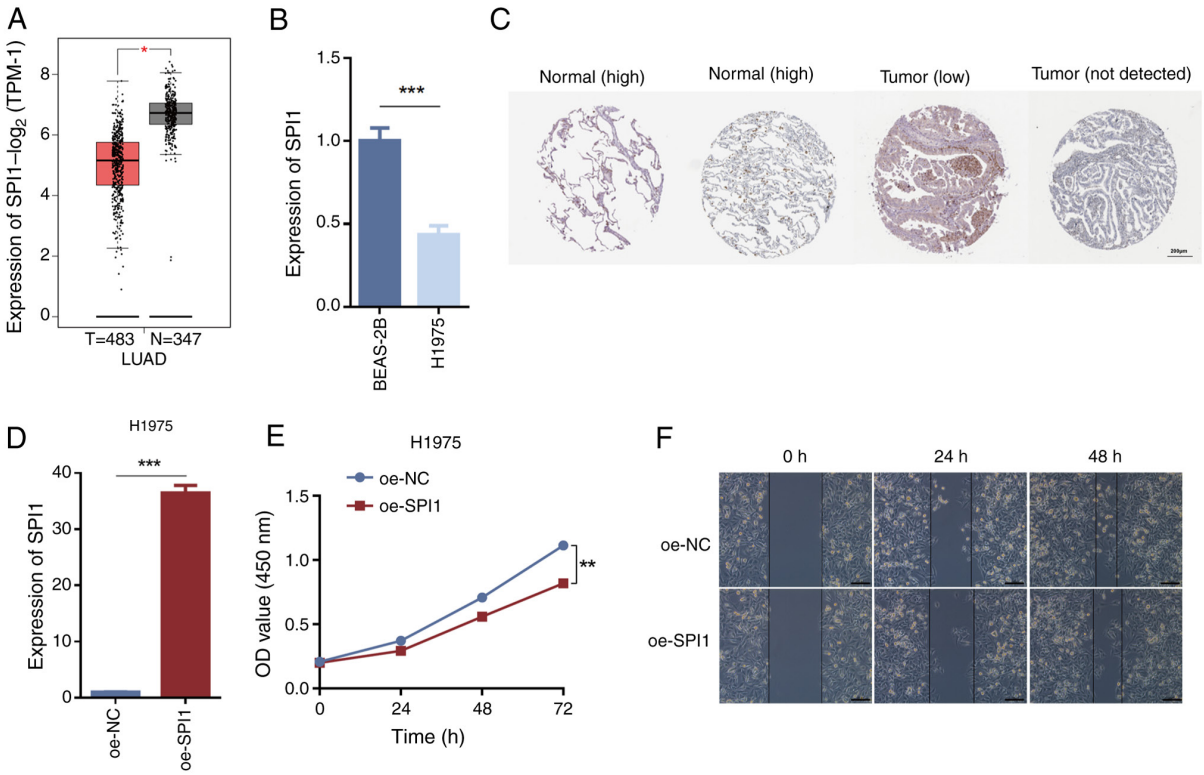

Figure 6. Transfection with oe-SPI1 significantly inhibits proliferation and migration in LUAD. (A) mRNA expression levels of SPI1 in LUAD (n=483) and normal (n=347) tissues. (B) RT-qPCR validation of the expression of SPI1 in normal and LUAD cell lines. (C) The Human Protein Atlas database (images available from v24.proteinatlas.org) revealed differences in SPI1 protein expression between normal tissues and LUAD tissues. (D) mRNA expression of SPI1 in cells transfected with oe-SPI1, assessed by RT-qPCR. (E) Cell Counting Kit-8 assay measuring the proliferative capacity of H1975 cells after oe-SPI1 transfection. (F) Wound healing assay demonstrating that the oe-SPI1 transfection inhibited the migration of H1975 tumor cell lines. *P<0.05; **P<0.01; ***P<0.001. SPI1, Spi-1 proto-oncogene; LUAD, lung adenocarcinoma; RT-qPCR, reverse transcription-quantitative polymerase chain reaction; oe, overexpression; NC, negative control.

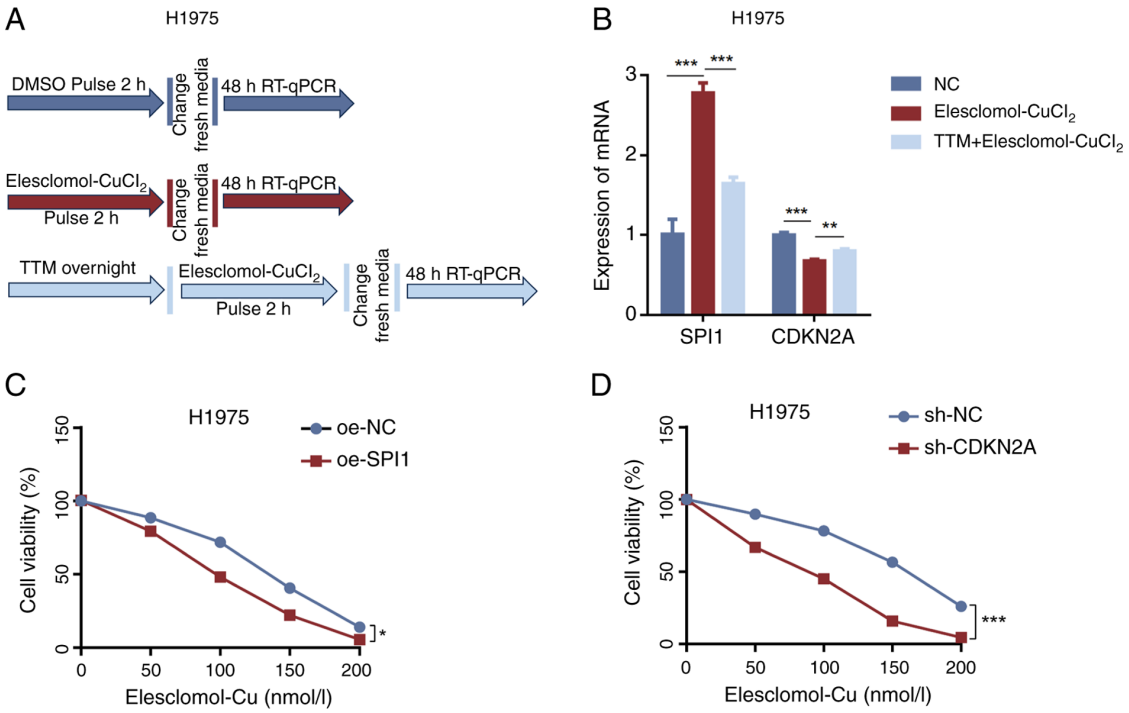

Figure 7. Association of SPI1 and CDKN2A with cell death induced by copper ionophore. (A) Schematic representation of the cuproptosis induction model. (B) Changes in mRNA expression levels detected by RT-qPCR 48 h after cuproptosis experimental treatment. H1975 cells were transfected with (C) oe-SPI1 or (D) sh-CDKN2A constructs and treated with the indicated concentrations of elesclomol-$CuCl_2$ for 72 h. Cell viability was measured using the cell counting Kit-8 assay. *P<0.05; **P<0.01; ***P<0.001. SPI1, SPI1 proto-oncogene; CDKN2A, CDK inhibitor 2A; RT-qPCR, reverse transcription-quantitative polymerase chain reaction; oe, overexpression; NC, negative control; sh, short hairpin; TTM, tetrathiomolybdate.

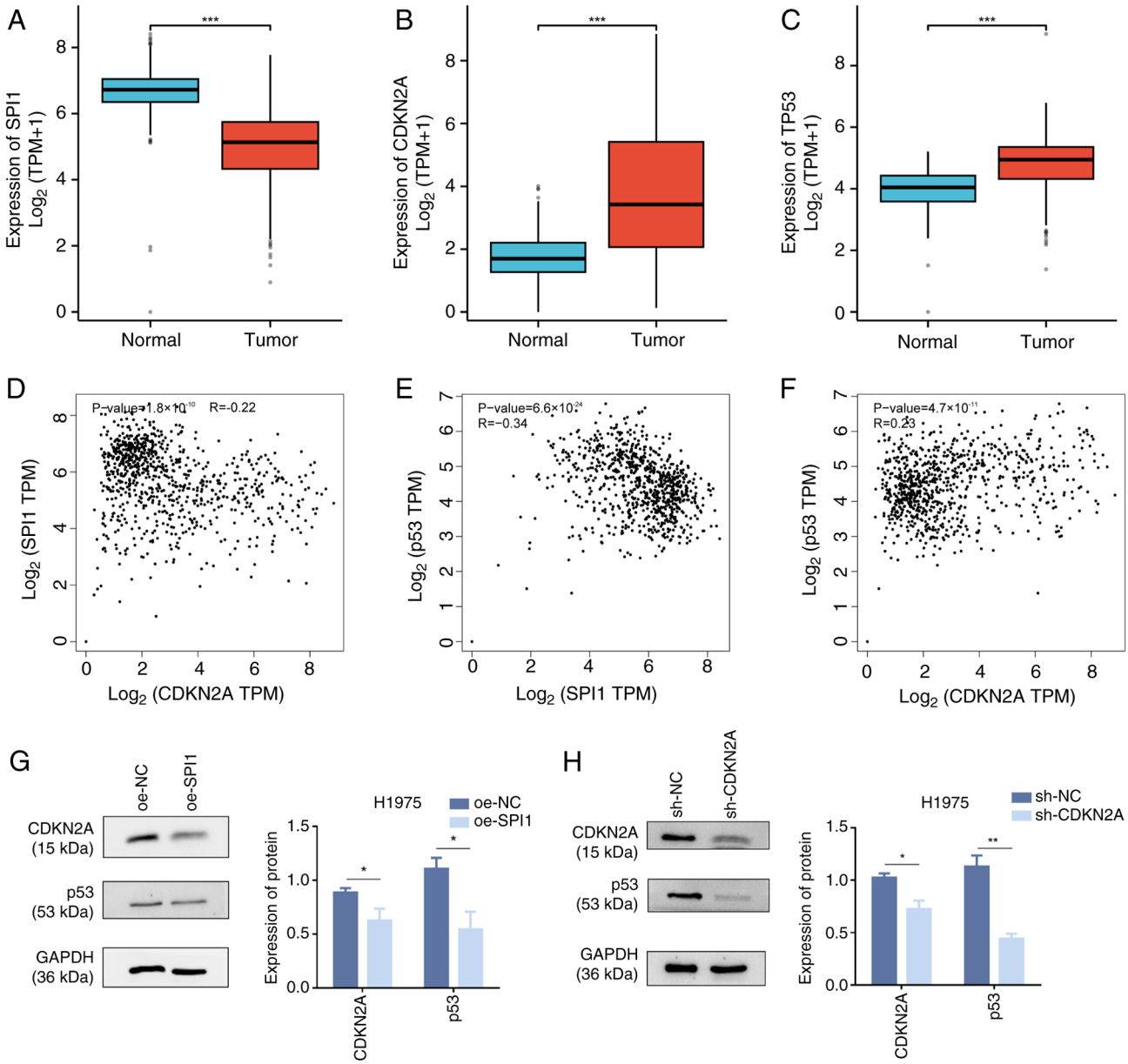

Figure 8. Regulation of cuproptosis in LUAD cells by the SPI1/CDKN2A/p53 signaling axis. Analysis of data from The Cancer Genome Atlas in conjunction with Genotype-Tissue Expression to validate the statistical significance of (A) SPI1, (B) CDKN2A and (C) TP53 in tumor (n=515) and normal (n=347) tissues. (D) Negative correlation between SPI1 and CDKN2A co-expression in LUAD, with an R value of -0.22. (E) Negative correlation between SPI1 and TP53 co-expression in LUAD, with an R value of -0.34. (F) Positive correlation between CDKN2A and TP53 co-expression in LUAD, with an R value of 0.23. (G) Western blot analysis of CDKN2A, p53 and GAPDH protein expression in H1975 cells following oe-SPI1 transfection. (H) Western blot analysis of p53 and GAPDH protein expression in H1975 cells after the knockdown of CDKN2A. *P<0.05; **P<0.01; ***P<0.001. LUAD, lung adenocarcinoma; SPI1, SPI1 proto-oncogene; CDKN2A, CDK inhibitor 2A; oe, overexpression; sh, short hairpin; NC, negative control; TPM, transcripts per million.

p53 protein levels (Fig. 8H). These findings suggested that SPI1 may promote the cuproptosis of LUAD cells. Whereas CDKN2A and p53 as anti-cuproptosis genes can inhibit the cuproptosis of LUAD, SPI1 can decrease the content of CDKN2A and p53 thereby affecting the cuproptosis of LUAD cells. Based on the discovered gene pathway association, SPI1 may promote cuproptosis in LUAD cells by negatively regulating CDKN2A and p53.

Discussion

Copper, a ubiquitous transition metal element, exhibits notable redox properties in its ionic form within biological systems. Copper ions participate in numerous biochemical reactions by donating or accepting electrons. Imbalances in copper ion concentrations can lead to oxidative stress reactions and abnormal autophagy, thereby triggering various copper- or copper ion-associated diseases, such as Menkes disease, Wilson's disease, neurodegenerative diseases, anemia, metabolic syndrome, cardiovascular diseases and cancer (7,40,41). Tsvetkov *et al* (8) proposed the concept of cuproptosis and identified 13 CRGs, with the primary targets including seven positive regulators: FDX1, LIAS, LIPT1, DLD, DLAT, PDHA1 and PDHB, and three negative regulators: MTF1, GLS, and CDKN2A. Previous research has explored the functions and importance of CRGs. For example, under the manipulation

of mitochondrial Fe-S cluster proteins and FDX1, excessive intracellular copper reduces Cu^{2+} to the highly toxic Cu^{+} form by participating in energy metabolism and DNA synthesis. ES, a copper ionophore, directly acts on FDX1 to facilitate efficient copper transport into cells. DLAT, a component of the PDH complex, promotes disulfide-dependent aggregation of lipoylated DLAT (42). The expression and mechanisms of CRGs in tumors are complex, and the functions of other CRGs remain to be elucidated.

The present study, through bioinformatics analysis, identified CDKN2A as a crucial gene in cuproptosis of LUAD, with SPI1 as its upstream cuproptosis-related TF and p53 as its downstream cuproptosis-related pathway. The expression and functions of relevant genes were validated through RT-qPCR, CCK-8 assays, western blotting and cuproptosis-related experiments. The high expression of CDKN2A in LUAD was associated with a poor prognosis for patients. CDKN2A is the most frequently somatically mutated cuproptosis regulator, and its abnormal status is associated with tumorigenesis and progression (43). CDKN2A is highly expressed in most tumor cells, and upregulation of this gene markedly affects the cell cycle and other cellular functions, potentially leading to cancer progression and poor prognosis for patients. This makes CDKN2A a potential prognostic biomarker (15,44,45), although the specific mechanisms underlying its association with poor prognosis remain unclear. Previous research reported that CDKN2A and MTF1 are cuproptosis-associated differential genes in LUAD, exhibiting differential expression across immune subtypes (45). The expression levels of CDKN2A and MTF1 are associated with various functional states of LUAD. Notably, CDKN2A demonstrates a negative association with survival prognosis in LUAD; therefore, intervention strategies targeting CDKN2A and MTF1 in LUAD, as well as potential combination therapies, should be the focus of future research endeavors (45). CDKN2A may adversely affect the prognosis of certain tumors by inhibiting cuproptosis activity and may be influenced by other cuproptosis-related regulators. Therefore, targeted therapy addressing multiple cuproptosis regulators, including CDKN2A, may yield notable synergistic effects. This hypothesis requires extensive basic and clinical research for validation (24). Previous studies have used the CCK-8 assay to measure cell viability at indicated time points after ES-Cu (1:1 ratio) pulse treatment in fresh medium, and to assess sensitivity of cells to ES-$CuCl_2$ after gene overexpression or knockdown (46-48). In the present study, after cuproptosis was induced with ES-$CuCl_2$, CDKN2A expression was downregulated, whereas pretreatment with TTM inhibited this downregulation. Additionally, knocking down CDKN2A increased the sensitivity of LUAD cells to cuproptosis. Further studies are needed to determine how CDKN2A regulates cellular cuproptosis.

SPI1, also known as PU.1, was identified as the upstream regulator of CDKN2A in LUAD cuproptosis. It was initially isolated by Moreau-Gachelin *et al* (49) from Friend erythroleukemia and belongs to the erythroblast transformation-specific family of TFs. Prior studies have demonstrated the tumor suppressor role of SPI1 in classical Hodgkin lymphoma cells and non-Hodgkin lymphoma cells by modulating the cell cycle and apoptosis (50,51). The present analysis highlighted the importance of SPI1 as a prognostic TF for CDKN2A in LUAD cuproptosis, by negatively regulating CDKN2A activity. SPI1 was identified as a common TF for CDKN2A and a cuproptosis gene set in LUAD, aligning with the findings of Huo *et al* (48), which demonstrated that the upregulation of SLC3A1, induced by ATF3/SPI1, facilitates the excessive accumulation of advanced glycation end products and copper in diabetic cardiomyocytes, thereby disrupting copper homeostasis and promoting cuproptosis. The Epstein-Barr virus nuclear antigen 3C binds to BATF/IRF4 or SPI1/IRF4 complex sites, thereby recruiting Sin3A to suppress CDKN2A; however, the direct regulatory mechanisms remain to be elucidated (52). Current research on the role of SPI1 in cuproptosis and LUAD is limited. However, predictive analyses across multiple databases identified transcriptional regulation of CDKN2A by SPI1, which was further assessed through western blotting. Upon ES-$CuCl_2$-induced cuproptosis, SPI1 expression was upregulated, whereas pretreatment with the copper chelator TTM suppressed this upregulation. Furthermore, cell proliferation assays demonstrated that SPI1 overexpression promoted ES-$CuCl_2$-induced cuproptosis, corroborating its role in LUAD cells.

The KEGG pathway enrichment analysis revealed the association of CDKN2A with cancer-associated pathways, including p53 signaling, DNA replication and cell cycle signaling. In >25 cancer types, cuproptosis is inversely associated with cellular mechanisms such as apical junctions, mitotic spindle function, epithelial-mesenchymal transition, transforming growth factor-β signaling and p53 function, suggesting its potential as a target for tumor metastasis and growth inhibition (24). The tumor suppressor p53 is a key metabolic regulator. Previous evidence has highlighted the role of p53 in reshaping cancer energy metabolism, mediating the shift from glycolysis to oxidative phosphorylation, enhancing Fe-S cluster biogenesis and coordinating copper chelator GSH levels. This finding indicated the dual function of p53 in promoting or inhibiting cuproptosis under various stress conditions. Mutant p53 enhances glycolysis, inhibits oxidative phosphorylation and modulates lipid metabolism through several mechanisms, potentially fortifying cancer cells against cuproptosis (53). As a central regulator of apoptosis by transcribing multiple apoptotic target genes, copper enhances the transcriptional activity of p53 to induce apoptosis (54). Furthermore, Tschan *et al* (55) found that SPI1 can impair the transcriptional activity of p53 by binding to specific regions, thereby modulating the cell cycle and apoptosis. The SPI1/CDKN2A/p53 regulatory network has notable implications for understanding tumorigenesis, cellular metabolism and cuproptosis, warranting further investigation.

In conclusion, the present study identified a signaling pathway regulating cuproptosis mechanisms in LUAD through the integration of public database resources, and validated it through cellular experiments. Furthermore, the specific role of the SPI1/CDKN2A/p53 signaling axis in modulating cuproptosis processes was evaluated in LUAD cells. The present study revealed that after copper induces cuproptosis in H1975 cells, SPI1 expression may be upregulated, whereas CDKN2A expression is downregulated. When H1975 cells were pretreated with TTM, the upregulation of SPI1 was revealed to be inhibited and the downregulation of CDKN2A was also suppressed. Based on gene pathway associations, SPI1 could promote cuproptosis in LUAD cells by inhibiting the expression of CDKN2A and p53.

Thus, the present study established a theoretical foundation for further explorations in the field of cuproptosis. Nonetheless, the present research relies on widely used public data resources and no clinical studies were performed. Furthermore, in addition to affecting CDKN2A and p53, and thus influencing cuproptosis in LUAD cells, other mechanisms of SPI1 on cuproptosis remain to be explored. Therefore, future endeavors should integrate clinical validations to ensure the comprehensiveness and accuracy of the findings, and the mechanisms underlying cuproptosis require further analysis.

Acknowledgements

Not applicable.

Funding

The present study was supported by The Natural Science Foundation of Shandong Province (grant no. ZR2023MH223), The National Natural Science Foundation of China (grant no. 32301062), The Shandong Province Medical and health science and Technology Plan (grant no. 202304020786) and The National College Students Innovation and Entrepreneurship Training Program (grant no. 202310440029).

Availability of data and materials

The data generated in the present study may be requested from the corresponding author.

Authors' contributions

YL and NX were involved in conceptualization. WS and SL performed the formal analysis. QW and XF performed analysis and interpretation of the data. WS and RW were involved in conception and design of the study. BT, XL and JA performed some experiments. JA and WS wrote the original draft. YL and NX confirm the authenticity of all the raw data. All authors read and approved the final version of the manuscript.

Ethical approval and consent to participate

Not applicable.

Patient consent for publication

Not applicable.

Competing interests

The authors declare that they have no competing interests.

References

1. Siegel RL, Giaquinto AN and Jemal A: Cancer statistics, 2024. CA Cancer J Clin 74: 12-49, 2024.
2. Chen P, Liu Y, Wen Y and Zhou C: Non-small cell lung cancer in China. Cancer Commun (Lond) 42: 937-970, 2022.
3. Jurisic V, Vukovic V, Obradovic J, Gulyaeva LF, Kushlinskii NE and Djordjević N: EGFR polymorphism and survival of NSCLC patients treated with TKIs: A systematic review and meta-analysis. J Oncol 2020: 1973241, 2020.
4. Jiao G and Wang B: NK cell subtypes as regulators of autoimmune liver disease. Gastroenterol Res Pract 2016: 6903496, 2016.
5. Brand A, Singer K, Koehl GE, Kolitzus M, Schoenhammer G, Thiel A, Matos C, Bruss C, Klobuch S, Peter K, *et al*: LDHA-associated lactic acid production blunts tumor immunosurveillance by T and NK cells. Cell Metab 24: 657-671, 2016.
6. Ma Q, Jiang H, Ma L, Zhao G, Xu Q, Guo D, He N, Liu H, Meng Z, Liu J, *et al*: The moonlighting function of glycolytic enzyme enolase-1 promotes choline phospholipid metabolism and tumor cell proliferation. Proc Natl Acad Sci USA 120: e2209435120, 2023.
7. Chen Y, Tang L, Huang W, Zhang Y, Abisola FH and Li L: Identification and validation of a novel cuproptosis-related signature as a prognostic model for lung adenocarcinoma. Front Endocrinol (Lausanne) 13: 963220, 2022.
8. Tsvetkov P, Coy S, Petrova B, Dreishpoon M, Verma A, Abdusamad M, Rossen J, Joesch-Cohen L, Humeidi R, Spangler RD, *et al*: Copper induces cell death by targeting lipoylated TCA cycle proteins. Science 375: 1254-1261, 2022.
9. Mou Y, Wang J, Wu J, He D, Zhang C, Duan C and Li B: Ferroptosis, a new form of cell death: Opportunities and challenges in cancer. J Hematol Oncol 12: 34, 2019.
10. D'Arcy MS: Cell death: A review of the major forms of apoptosis, necrosis and autophagy. Cell Biol Int 43: 582-592, 2019.
11. Fang Y, Tian S, Pan Y, Li W, Wang Q, Tang Y, Yu T, Wu X, Shi Y, Ma P and Shu Y: Pyroptosis: A new frontier in cancer. Biomed Pharmacother 121: 109595, 2020.
12. Su Z, Yang Z, Xu Y, Chen Y and Yu Q: Apoptosis, autophagy, necroptosis, and cancer metastasis. Mol Cancer 14: 48, 2015.
13. Tsvetkov P, Detappe A, Cai K, Keys HR, Brune Z, Ying W, Thiru P, Reidy M, Kugener G, Rossen J, *et al*: Mitochondrial metabolism promotes adaptation to proteotoxic stress. Nat Chem Biol 15: 681-689, 2019.
14. Huang Y, Yin D and Wu L: Identification of cuproptosis-related subtypes and development of a prognostic signature in colorectal cancer. Sci Rep 12: 17348, 2022.
15. Liu H and Tang T: Pan-cancer genetic analysis of cuproptosis and copper metabolism-related gene set. Front Oncol 12: 952290, 2022.
16. Da Silva DA, De Luca A, Squitti R, Rongioletti M, Rossi L, Machado CML and Cerchiaro G: Copper in tumors and the use of copper-based compounds in cancer treatment. J Inorg Biochem 226: 111634, 2022.
17. Salem A, Ahmed S, Khalfallah M, Hamadan N, ElShikh W and Alfaki M: A comprehensive pan-cancer analysis reveals cyclin-dependent kinase inhibitor 2A gene as a potential diagnostic and prognostic biomarker in colon adenocarcinoma. Cureus 16: e60586, 2024.
18. Stott FJ, Bates S, James MC, McConnell BB, Starborg M, Brookes S, Palmero I, Ryan K, Hara E, Vousden KH and Peters G: The alternative product from the human CDKN2A locus, p14(ARF), participates in a regulatory feedback loop with p53 and MDM2. EMBO J 17: 5001-5014, 1998.
19. Liu MT, Liu JY and Su J: CDKN2A gene in melanoma. Zhonghua Bing Li Xue Za Zhi 48: 909-912, 2019 (In Chinese).
20. Chen Y: Identification and validation of cuproptosis-related prognostic signature and associated regulatory axis in uterine corpus endometrial carcinoma. Front Genet 13: 912037, 2022.
21. Zhou Z, Zhou Y, Liu D, Yang Q, Tang M and Liu W: Prognostic and immune correlation evaluation of a novel cuproptosis-related genes signature in hepatocellular carcinoma. Front Pharmacol 13: 1074123, 2022.
22. Shi WK, Li YH, Bai XS and Lin GL: The cell cycle-associated protein CDKN2A may promotes colorectal cancer cell metastasis by inducing epithelial-mesenchymal transition. Front Oncol 12: 834235, 2022.
23. Zhang D, Wang T, Zhou Y and Zhang X: Comprehensive analyses of cuproptosis-related gene CDKN2A on prognosis and immunologic therapy in human tumors. Medicine (Baltimore) 102: e33468, 2023.
24. Wu C, Tan J, Wang X, Qin C, Long W, Pan Y, Li Y and Liu Q: Pan-cancer analyses reveal molecular and clinical characteristics of cuproptosis regulators. Imeta 2: e68, 2022.
25. Tomczak K, Czerwińska P and Wiznerowicz M: The cancer genome atlas (TCGA): An immeasurable source of knowledge. Contemp Oncol (Pozn) 19: A68-77, 2015.
26. RStudio Team. RStudio: Integrated Development for R. RStudio, PBC, Boston, MA, 2020. http://www.rstudio.com/. Accessed October 15, 2023.

27. Shen W, Song Z, Zhong X, Huang M, Shen D, Gao P, Qian X, Wang M, He X, Wang T, *et al*: Sangerbox: A comprehensive, interaction-friendly clinical bioinformatics analysis platform. Imeta 1: e36, 2022.
28. Law CW, Chen Y, Shi W and Smyth GK: voom: Precision weights unlock linear model analysis tools for RNA-seq read counts. Genome Biol 15: R29, 2014.
29. Szklarczyk D, Gable AL, Nastou KC, Lyon D, Kirsch R, Pyysalo S, Doncheva NT, Legeay M, Fang T, Bork P, *et al*: The STRING database in 2021: Customizable protein-protein networks, and functional characterization of user-uploaded gene/measurement sets. Nucleic Acids Res 49 (D1): D605-D612, 2021.
30. Doncheva NT, Morris JH, Gorodkin J and Jensen LJ: Cytoscape StringApp: Network analysis and visualization of proteomics data. J Proteome Res 18: 623-632, 2019.
31. Chin CH, Chen SH, Wu HH, Ho CW, Ko MT and Lin CY: cytoHubba: Identifying hub objects and sub-networks from complex interactome. BMC Syst Biol 8 (Suppl 4): S11, 2014.
32. Tang Z, Kang B, Li C, Chen T and Zhang Z: GEPIA2: An enhanced web server for large-scale expression profiling and interactive analysis. Nucleic Acids Res 47 (W1): W556-W560, 2019.
33. Uhlén M, Fagerberg L, Hallström BM, Lindskog C, Oksvold P, Mardinoglu A, Sivertsson Å, Kampf C, Sjöstedt E, Asplund A, *et al*: Proteomics. Tissue-based map of the human proteome. Science 347: 1260419, 2015.
34. Chandrashekar DS, Bashel B, Balasubramanya SAH, Creighton CJ, Ponce-Rodriguez I, Chakravarthi BVSK and Varambally S: UALCAN: A portal for facilitating tumor subgroup gene expression and survival analyses. Neoplasia 19: 649-658, 2017.
35. Nagy Á, Munkácsy G and Győrffy B: Pancancer survival analysis of cancer hallmark genes. Sci Rep 11: 6047, 2021.
36. Vasaikar SV, Straub P, Wang J and Zhang B: LinkedOmics: Analyzing multi-omics data within and across 32 cancer types. Nucleic Acids Res 46 (D1): D956-D963, 2018.
37. Kanehisa M, Araki M, Goto S, Hattori M, Hirakawa M, Itoh M, Katayama T, Kawashima S, Okuda S, Tokimatsu T and Yamanishi Y: KEGG for linking genomes to life and the environment. Nucleic Acids Res 36 (Database Issue): D480-D484, 2008.
38. Wang S and Liu X: The UCSCXenaTools R package: A toolkit for accessing genomics data from UCSC Xena platform, from cancer multi-omics to single-cell RNA-seq. J Open Source Softw 4: 1627, 2019.
39. Livak KJ and Schmittgen TD: Analysis of relative gene expression data using real-time quantitative PCR and the 2(-Delta Delta C(T)) method. Methods 25: 402-408, 2001.
40. Linder MC and Hazegh-Azam M: Copper biochemistry and molecular biology. Am J Clin Nutr 63: 797S-811S, 1996.
41. Li Y and Trush MA: DNA damage resulting from the oxidation of hydroquinone by copper: Role for a Cu(II)/Cu(I) redox cycle and reactive oxygen generation. Carcinogenesis 14: 1303-1311, 1993.
42. Duan WJ and He RR: Cuproptosis: Copper-induced regulated cell death. Sci China Life Sci 65: 1680-1682, 2022.
43. Wang H, Liu J, Zhu S, Miao K, Li Z, Qi X, Huang L, Guo L, Wang Y, Cai Y and Lin Y: Comprehensive analyses of genomic features and mutational signatures in adenosquamous carcinoma of the lung. Front Oncol 12: 945843, 2022.
44. Ichikawa K, Imura J, Kawamata H, Takeda J and Fujimori T: Down-regulated p16 expression predicts poor prognosis in patients with extrahepatic biliary tract carcinomas. Int J Oncol 20: 453-461, 2002.
45. Li M, Tan Y, Li Z and Min L: Biological characterization and clinical significance of cuproptosis-related genes in lung adenocarcinoma. BMC Pulm Med 25: 13, 2025.
46. Yu YH, Li HJ, Yang XY, Yu LY and Tong XM: Elesclomol-Cu induces cuproptosis in human acute myeloid leukemia cells. Zhongguo Shi Yan Xue Ye Xue Za Zhi 32: 389-394, 2024.
47. Chen Y, Tang L, Huang W, Abisola FH, Zhang Y, Zhang G and Yao L: Identification of a prognostic cuproptosis-related signature in hepatocellular carcinoma. Biol Direct 18: 4, 2023.
48. Huo S, Wang Q, Shi W, Peng L, Jiang Y, Zhu M, Guo J, Peng D, Wang M, Men L, *et al*: ATF3/SPI1/SLC31A1 signaling promotes cuproptosis induced by advanced glycosylation end products in diabetic myocardial injury. Int J Mol Sci 24: 1667, 2023.
49. Moreau-Gachelin F, Tavitian A and Tambourin P: Spi-1 is a putative oncogene in virally induced murine erythroleukaemias. Nature 331: 277-280, 1988.
50. Yuki H, Ueno S, Tatetsu H, Niiro H, Iino T, Endo S, Kawano Y, Komohara Y, Takeya M, Hata H, *et al*: PU.1 is a potent tumor suppressor in classical Hodgkin lymphoma cells. Blood 121: 962-970, 2013.
51. Endo S, Nishimura N, Toyoda K, Komohara Y, Carreras J, Yuki H, Shichijo T, Ueno S, Ueno N, Hirata S, *et al*: Decreased PU.1 expression in mature B cells induces lymphomagenesis. Cancer Sci 115: 3890-3901, 2024.
52. Jiang S, Willox B, Zhou H, Holthaus AM, Wang A, Shi TT, Maruo S, Kharchenko PV, Johannsen EC, Kieff E and Zhao B: Epstein-Barr virus nuclear antigen 3C binds to BATF/IRF4 or SPI1/IRF4 composite sites and recruits Sin3A to repress CDKN2A. Proc Natl Acad Sci USA 111: 421-426, 2014.
53. Xiong C, Ling H, Hao Q and Zhou X: Cuproptosis: p53-regulated metabolic cell death? Cell Death Differ 30: 876-884, 2023.
54. Xue Q, Kang R, Klionsky DJ, Tang D, Liu J and Chen X: Copper metabolism in cell death and autophagy. Autophagy 19: 2175-2195, 2023.
55. Tschan MP, Reddy VA, Ress A, Arvidsson G, Fey MF and Torbett BE: PU.1 binding to the p53 family of tumor suppressors impairs their transcriptional activity. Oncogene 27: 3489-3493, 2008.